

**Key Points:**

- South American summer monsoon variability is influenced by multidecadal and interannual variability of Pacific sea surface temperatures
- Paleoclimate records combined with climate model synthesis enhance the interpretation of Pacific Ocean–South America teleconnections
- The development of new paleoclimate records in South America can be informed by the archived signals of Pacific multidecadal variability

Supporting Information:

Supporting Information may be found in the online version of this article.

Correspondence to:

R. Orrison,
orrison@albany.edu

Citation:

Orrison, R., Vuille, M., Rodrigues, J. C., Strikis, N. M., Cruz, F., Rodriguez-Caton, M., & Andreu-Hayles, L. (2024). Pacific interannual and multidecadal variability recorded in $\delta^{18}\text{O}$ of South American Summer Monsoon precipitation. *Journal of Geophysical Research: Atmospheres*, 129, e2024JD040999. <https://doi.org/10.1029/2024JD040999>

Received 12 FEB 2024

Accepted 25 AUG 2024

Pacific Interannual and Multidecadal Variability Recorded in $\delta^{18}\text{O}$ of South American Summer Monsoon Precipitation

R. Orrison¹ , M. Vuille¹ , J. C. Rodrigues², N. M. Strikis³ , F. Cruz³, M. Rodriguez-Caton^{4,5} , and L. Andreu-Hayles^{6,7,8} 

¹Department of Atmospheric and Environmental Sciences, University at Albany, Albany, NY, USA, ²Institute for Geosciences, Johannes Gutenberg University Mainz, Mainz, Germany, ³Instituto de Geociências, Universidade de São Paulo (USP), São Paulo, Brazil, ⁴Instituto Argentino de Nivología, Glaciología y Ciencias Ambientales, CCT CONICET Mendoza, Mendoza, Argentina, ⁵Department of Plant Sciences, University of California Davis, Davis, CA, USA, ⁶Lamont-Doherty Earth Observatory of Columbia University, Palisades, NY, USA, ⁷CREAF, Barcelona, Spain, ⁸ICREA, Barcelona, Spain

Abstract The South American summer monsoon (SASM) generates important hydroclimatic impacts in (sub-)tropical South America and isotopic tracers recorded in paleoclimatic archives allow for assessing its long-term response to Pacific variability prior to modern observations. Stable oxygen isotopes in precipitation integrate hydroclimatic changes during the SASM mature phase from December to February (DJF) in response to the Interdecadal Pacific Oscillation (IPO) and El Niño—Southern Oscillation (ENSO), respectively. Here, results from the isotope-enabled Community Atmosphere Model v.5 are compared with highly resolved and precisely dated isotopic records from speleothems, tree rings, lake and ice cores during the industrial era (1880–2000 CE) and validated against observations from the International Atomic Energy Agency (IAEA) network. Pacific sea surface temperatures (SSTs) are coupled to the isotopic composition of SASM precipitation through perturbations in the Walker circulation associated with low- (IPO) and high-frequency (ENSO) variability, impacting convective activity over tropical South America and the tropical Atlantic. Changes in convection over this monsoon entrance region ultimately control the downstream oxygen isotopic composition of precipitation recorded in paleoclimate archives. Overall, model results, paleoclimate records and IAEA data agree on the isotopic response to Pacific SST forcing. These results highlight the potential for long isotopic paleoclimate records to reconstruct Pacific climate variability on both high- and low-frequency timescales. Furthermore, the isolation of the IPO signal in a diverse set of isotopic archives invites the reinterpretation of other paleoclimate proxies for identifying this historically overlooked forcing.

Plain Language Summary The summertime rainfall associated with the South American monsoon is important for the hydropower and agricultural sectors in South America as well as to the traditions of many Amazonian indigenous cultures. The amount and spatial extent of the monsoon rainfall patterns are influenced by a variety of factors, including changes in Pacific Ocean sea surface temperatures. While evaluating this link has been mostly limited to meteorological observations, the analysis of heavy and light oxygen atoms, called isotopes, in natural archives such as cave deposits, lake sediments, glacier ice, and tree rings, can help extend this relationship further back in time. In combination with climate models, the ratio between heavy and light isotopes can provide insight for the link between the Pacific Ocean and South American water cycle changes on interannual to multidecadal timescales. This allows us to better understand how the Pacific has influenced the South American monsoon in the past. It also allows us to better define the range of natural climate variability against which future changes can be compared.

1. Introduction

The South American summer monsoon (SASM) is the main dynamic feature associated with interannual rainfall variability in tropical and subtropical South America (Marengo et al., 2012; Vera et al., 2006). Monsoon rainfall is crucial to water management, energy generation, livelihoods of traditional rural communities and indigenous practices across the region. SASM-related convection over the Amazon basin results in the development of the Bolivian High-Nordeste Low system (Chen et al., 1999; Lenters & Cook, 1997), with convection over the western Amazon balanced by subsidence over northeastern Brazil (also known as the “Nordeste” region) and the adjacent subtropical Atlantic, setting up a west-east hydrologic dipole (Sulca et al., 2016). This dipole pattern peaks in the

austral summer (December, January and February; DJF) and leads to rainy conditions along the eastern flank of the tropical Andes and the central-western Amazon basin, while dry conditions prevail over the easternmost Amazon, northeastern and central Brazil. In southeastern Brazil, the summertime brings intense local rainfall within the South Atlantic Convergence Zone (SACZ) and precipitation is fueled by moisture transported southeastward by the South American low-level jet, uplifted by the baroclinic instability from the convergence of anticyclonic flow from the South Atlantic Anticyclone and transient cold waves breaking northward off the mid-level jet. These features of the SASM system have been recorded across timescales (e.g., Cruz et al., 2009; Novello et al., 2012) and captured by diverse proxy records as regional isotopic signals (Campos et al., 2019; Orrison et al., 2022; Vuille et al., 2012). The mean state of the monsoon system is, however, modulated by internal variability of the tropical Pacific on multiple timescales. A mechanistic diagnosis of how oxygen isotope paleoclimate records archive the SASM sensitivity to Pacific variability will help assess their potential for both monsoon and Pacific climate reconstruction on interannual to multidecadal timescales. Documenting the influence of the Pacific on tropical South American hydroclimate over the past century also yields an important benchmark for isolating internal variability against which future externally forced change can be compared.

Modes of interannual and multidecadal sea surface temperature (SST) variability in the Pacific are important modulators of hydroclimate variability in South America (Cai et al., 2020; Garreaud et al., 2009; Sulca et al., 2018). High-frequency variability is associated with the El Niño—Southern Oscillation (ENSO), identified as varying on 2–7 years timescales and indexed by capturing tropical Pacific SST anomalies. ENSO is the leading mode of Pacific SST variability and has strong teleconnections with significant hydroclimate impacts over South America (Cai et al., 2020). Low-frequency variability in the Pacific, while subject to broader interpretation, has been defined as a mode of basin-wide SST variability known as the Interdecadal Pacific Oscillation (IPO). The IPO has also been linked to hydroclimate variability at a global scale (Buckley et al., 2019; Porter et al., 2021; Vance et al., 2022).

The influence of ENSO on the oxygen isotopic composition of precipitation ($\delta^{18}\text{O}_\text{p}$) in the South American monsoon region has been well documented in several studies (Bradley et al., 2003; Hurley et al., 2019; Rodriguez-Caton et al., 2022; Vuille & Werner, 2005). Discrete paleoclimate records of $\delta^{18}\text{O}_\text{p}$ across the monsoon domain are positively correlated with high-frequency variability of Pacific SSTAs, such as in tree-ring cellulose records from the Amazon and the tropical Andes (Baker et al., 2022; Rodriguez-Caton et al., 2022) and in the Quelccaya ice core from the Peruvian Andes (Hurley et al., 2019; Thompson et al., 2013). Negative correlations between $\delta^{18}\text{O}_\text{p}$ and high-frequency Pacific SSTAs have been recorded in paleoclimate records from southeastern Brazil (Cauhy Rodrigues et al., 2022). Independently, $\delta^{18}\text{O}_\text{p}$ observations from the International Atomic Energy Agency (IAEA) network and early generation isotope-enabled climate models agree with paleoclimate records, with positive correlations between tropical Pacific SSTAs and $\delta^{18}\text{O}_\text{p}$ across the core of the Amazon basin, while negative correlations dominate along the coast of central-eastern Brazil (Vuille, Bradley, Werner, et al., 2003). Analyses with a fully coupled isotope-enabled climate model do show a relationship between ENSO and pseudoproxy models of $\delta^{18}\text{O}_\text{p}$ in paleoclimate records over South America, though with a limited network of sites in South America and the SASM region (Midhun et al., 2021). However, developing a high-density network with well-constrained and precisely dated paleoclimate records on interannual timescales is important to capture a coherent basin-wide response and synthesize previous studies. New tree-ring records, for example, show promise for revisiting the monsoon rainfall response to ENSO modes (Baker et al., 2022; Rodriguez-Caton et al., 2022) as well as decadal teleconnections between Altiplano region precipitation and central Pacific SSTs (Rodriguez-Caton et al., 2024).

Despite the importance of stable oxygen isotope ($\delta^{18}\text{O}$) paleoclimate records as a critical archive for documenting the past climate of South America, the isotopic response to changes in the IPO phase over South America is less well understood and has yet to be evaluated from a climatological and mechanistic perspective. This presents a critical gap in our understanding of the role this low-frequency mode plays in driving South American hydroclimate, particularly the SASM. Midhun et al. (2021) utilized a fully coupled climate model to evaluate the oxygen isotope response to multidecadal changes associated with the North Pacific (Pacific Decadal Oscillation) and Atlantic (Atlantic Multidecadal Oscillation) Oceans, leaving open the question of how a model constrained by observed SST might compare against paleoclimate records. The use of paleoclimate records spanning multiple positive and negative phases of multidecadal variability, such as exist from the South American Monsoon region, could be particularly insightful. Diagnosing to what extent isotopic proxies are able to capture Pacific low-

frequency variability is of key importance given the rapidly expanding network of high-resolution and precisely dated isotopic archives in the region (Campos et al., 2019; Orrison et al., 2022).

The physical processes by which environmental signals are encoded as $\delta^{18}\text{O}$ proxy data are archive-dependent and must be treated with care; uncertainty inherent to these processes imparts an intrinsic low-frequency filter to the paleoclimate records themselves. For example, isotopic diffusion in ice core records blends signal years (Evans et al., 2013) and reservoirs in aquifers above karstic cave systems increase water residence and mixing time periods (Moquet et al., 2016). These processes are likely to complicate the identification of high-frequency signals associated with ENSO, which require accurate and precise dating, high temporal resolution and detection of clear annual isotopic signals. To what extent such processes could also blur multidecadal signals is not clear. Therefore, establishing the extent to which these isotopic paleoclimate records can capture an IPO signal and to what extent such relationships can be adequately simulated by isotope-enabled climate models is critical to advance the interpretation and development of new low-frequency isotopic proxy records.

Here we synthesize $\delta^{18}\text{O}$ data from diverse data sources over a 120-year period to present a fresh perspective on the South American hydroclimate response to multiple phases of low-frequency Pacific variability as well as an updated assessment of the spatial response of $\delta^{18}\text{O}_\text{p}$ to high-frequency Pacific variability.

2. Hydroclimate Impacts of Pacific SST Modes

A variety of mechanisms contribute to Pacific modulation of South American hydroclimate. The perturbation of the Walker circulation in response to anomalously warmer or colder Pacific SSTs results in anomalous SASM convection and rainfall (Marengo & Espinoza, 2016). Precipitation changes associated with low-frequency variability exhibit a similar pattern compared to the high-frequency response, though with reduced amplitudes (Garreaud et al., 2009). During El Niño events, anomalous subsidence and reduction of cloud cover and moisture convergence have been found to reduce precipitation over the Amazon basin and northeastern Brazil, while the inverse is true during La Niña events (Cai et al., 2020; Grimm, 2003; Ronchail et al., 2002). Conversely, positive precipitation anomalies occur during the positive ENSO phase in southeastern South America (SESA) and along the tropical west coast of South America (Cai et al., 2020; Garreaud et al., 2009). This pattern is seen on multidecadal timescales as well, with a reduction in the convective intensity and rainfall over the Amazon during the positive phase of the IPO and the inverse during the negative IPO phase (He et al., 2021). The SACZ shifts slightly to the south during the positive IPO phase and more strongly to the north during the negative IPO phase (Silva et al., 2020). Though many features of the SASM rainfall response to Pacific SST anomalies (SSTAs) are consistent between the IPO and ENSO modes, the analysis of the IPO impacts over South America has been restricted by the limited availability of instrumental observations.

The South American hydroclimate response to Pacific SST patterns is dependent on a variety of contributing factors. Precipitation anomalies over South America vary seasonally (Dong et al., 2018; Garreaud et al., 2009) and depend on the background state of both Pacific and Atlantic high- and low-frequency oceanic modes, such as various flavors of ENSO (Sulca, 2021), the IPO, and Atlantic interannual and multidecadal variability (Cai et al., 2020; Dong et al., 2018; He et al., 2021; Meehl et al., 2021). For example, convection and precipitation anomalies associated with the Walker circulation over tropical South America have been shown to be damped when the Atlantic Multidecadal Oscillation (AMO) is in the opposite phase of ENSO (He et al., 2021; Kayano & Capistrano, 2014). Finally, joint impacts driven by coupled interactions between the Pacific and Atlantic further complicate the attribution of the various influences of these two ocean basins on hydroclimate and atmospheric circulation over South America (He et al., 2021).

3. Data and Methods

This study synthesizes climate model data, proxy records, and observational data, finding complementary intersections of these data sources to evaluate shared and disparate signals. The study is conducted over a 120-year period (1880–1999 Common Era (CE)), bounded by data availability and the lack of coherence in historical observations of SSTs prior to this period (Yasunaka & Hanawa, 2011). The extended period encompasses multiple positive and negative IPO phases and makes use of an extensive network of paleoclimatological records available during this period from the SASM domain across tropical and subtropical South America. We focus on the austral summer (December, January, and February ($D(t_0)J(t_{+1})F(t_{+1})$)), which corresponds to both the mature phase of the monsoon and the phase-locked peak of ENSO.

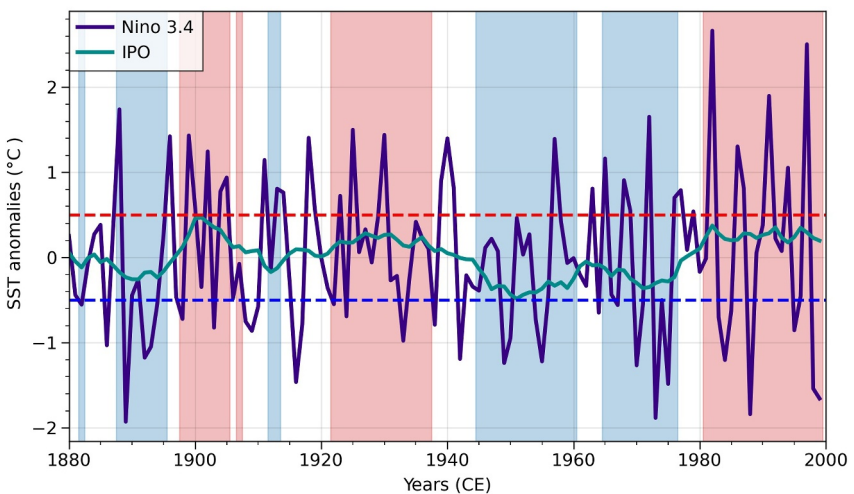


Figure 1. Indices of Pacific SSTA variability for the IPO (annual index) and ENSO (DJF index) (1880–2000 CE, Hadley OI-SST). Shaded bars indicate years when the IPO crosses the phase threshold with red (blue) shading indicating the IPO positive (negative) phase. The thresholds for ENSO positive/negative phases are indicated by the dashed blue and red lines ($\pm 0.5^{\circ}\text{C}$).

3.1. Model Simulations and Pacific Indices (IPO, ENSO)

The model data used for this study is from the isotope-enabled Community Atmosphere Model version 5 (iCAM5) simulation covering the Last Millennium (Nusbaumer et al., 2017). The iCAM5 simulation was run at a $0.9^{\circ} \times 1.25^{\circ}$ horizontal resolution with 30 vertical levels and was coupled to the isotope-enabled Community Land Model (iCLM4.0) (Wong et al., 2017). The experiment was constrained by a prescribed SST field using the Hadley Center-NOAA/OI Sea Surface Temperature (Hadley-OI SST) product, interpolated to $\sim 1.0^{\circ}$ horizontal resolution (Hurrell et al., 2008). Thus, the model response to SST-forced variability is well-suited for a historical comparison between model simulations, proxies and observations. This data set was also used to calculate indices of IPO and ENSO variability for the same period of study.

The South American isotopic hydroclimate response to low-frequency (multidecadal) Pacific variability, or IPO variability, was characterized by the Tripole Index (TPI) (Henley et al., 2015) (Figure 1). The TPI is defined as the average SST anomalies from a tropical region (10°S – 10°N , 170°E – 90°W) minus the average from two extratropical regions (25°N – 45°N , 140°E – 145°W ; 50°S – 15°S , 150°E – 160°W) (illustrated in Figure 2a). For each grid cell, the long-term trend was regressed out of the Hadley-OI SST data (Hurrell et al., 2008) and monthly residuals were averaged over the specified regions. Calendar year (January–December) averages, which are very similar to DJF averages due to the slow evolution of the SST anomalies, were calculated and an 11-year smoothing was applied to the timeseries to filter out high-frequency variability (He et al., 2021). Positive and negative phases of the IPO are defined as periods when the index passes the threshold of greater than/less than or equal to ± 0.5 standard deviations (based on He et al., 2021) (Table 1). For comparison between the IPO and DJF-only hydroclimate indices, the IPO year corresponds to the December month of the DJF season.

An index of high-frequency Pacific variability based on the Niño3.4 (N3.4) region (5°S – 5°N , 170°W – 120°W) (illustrated in Figure 2a) was calculated using December, January and February SSTAs, which were averaged to create a seasonal index (Figure 1). ENSO phases were selected using a modification of the NOAA Climate Prediction Center criteria based solely on the seasonal DJF N3.4 index crossing a threshold of greater than/less than or equal to $\pm 0.5^{\circ}\text{C}$ (Table 1). Other ENSO indices (Niño1+2, Niño3, and Niño4) were also analyzed and results were found to be similar to the N3.4 index (not shown).

3.2. South American $\delta^{18}\text{O}$ and Precipitation Data

Model simulations of hydroclimate impacts during both positive and negative phases of IPO and ENSO were validated with two distinct networks of DJF $\delta^{18}\text{O}$ variability: terrestrial paleoclimate records capturing monsoon

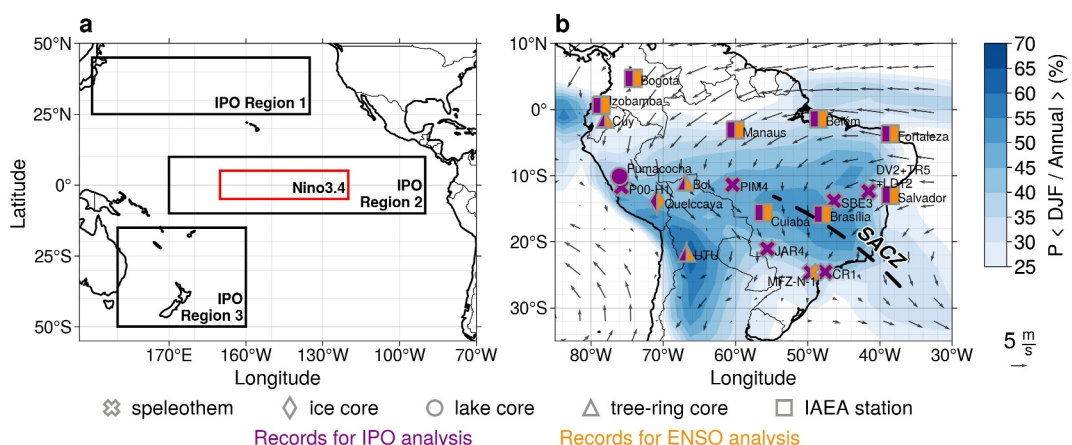


Figure 2. (a) Spatial domains used for the calculation of the TPI (characterizing IPO variability) and the N3.4 index and (b) networks of paleoclimate and IAEA $\delta^{18}\text{O}$ records over the SASM domain. Color shading in (b) represents the percent of water year (July–June) precipitation falling during the austral summer (DJF) period (GPCC, 1979–2019 CE). Vectors in (b) show the low-level wind field (850 hPa; ERA5, 1979–2020 CE). Symbols in (b) indicate different archive types (cross: speleothem; diamond: ice core; circle: lake core; triangle: tree-ring core; and square: IAEA station) and mark the approximate locations of IAEA stations and paleoclimate records used for the IPO analysis (indicated with purple color) and ENSO analysis (indicated with orange color). Pumacocha, P00-H1, and CR1 records are shifted slightly for better visibility.

rainfall and station observations from the IAEA Global Network of Isotopes in Precipitation (GNIP) (IAEA/WMO, 2023) (Figure 2; Table 2).

The records used to evaluate IPO and ENSO impacts were selected based on their published original interpretation of representing SASM variability. A subset of records from the full network was selected to evaluate ENSO impacts, since some proxy archival processes prevent a meaningful high-frequency interpretation of isotopic data. Only those records which record an annual $\delta^{18}\text{O}_\text{p}$ signal with fidelity (both in terms of data sampling resolution and precise and accurate annual age control) were utilized to evaluate the interannual ENSO signal within the SASM domain, as an age that is offset by one or 2 years will result in the difference between a positive or negative phase. This criteria is immediately inclusive of the selected tree-ring records, where isotopes in one ring of growth directly reflect the signal of the current growing season corresponding to the austral summer (Rodríguez-Catón et al., 2021) and where dating assigned to the calendar year in which growth began is both precise and accurate (Schulman, 1956). However, these limitations exclude most speleothems, as accurate dating, temporal resolution, and signal mixing processes related to aquifer mixing and internal epikarst systems all impart an environmental “low-pass” filter that smooths the archived climate signal. An exception to this is the use of the MFZ-N-1 speleothem, which exhibits rapid growth and a well-established age chronology (Cauhy Rodrigues et al., 2022). As a result, fewer speleothem records are available to analyze ENSO variability. The Pumacocha lake sediment record, while annually resolved, has been published as a decadal- to centennial-scale record and its interannual climate signal has not been explored as dating uncertainties of more than 1 year preclude its use for our ENSO analysis.

However, the effective low-pass filtering discussed here does not affect paleoclimate record suitability for detection of low-frequency forcings such as the IPO, where environmental or chronological offsets shifting

Table 1

IPO and ENSO Positive and Negative Phase Years During the Period of Study

Mode	Positive phase	Negative phase
IPO	1898–1905, 1907, 1922–1937, 1981–1999	1882, 1888–1895, 1912, 1913, 1945–1960, 1965–1976
ENSO	1888, 1896, 1899, 1900, 1902, 1904, 1905, 1911, 1913, 1914, 1918, 1919, 1923, 1925, 1930, 1939–1941, 1957, 1963, 1965, 1968, 1969, 1972, 1976, 1977, 1979, 1982, 1986, 1987, 1991, 1994, 1997	1882, 1886, 1889, 1892–1894, 1898, 1903, 1908–1910, 1916, 1917, 1922, 1924, 1933, 1938, 1942, 1949, 1950, 1954, 1955, 1964, 1967, 1970, 1971, 1973–1975, 1983–1985, 1988, 1995, 1998, 1999

Note. ENSO phase year refers to the December month in the DJF season.

Table 2
Terrestrial Archives of $\delta^{18}\text{O}$ Used in the IPO and ENSO Analysis

Sample ID	Record site	Archive	Sampling resolution	Location	Elevation (above sea level)	IPO	ENSO	Reference
Cuy	Cuyuja	Cedrela montana tree-ring cellulose	1 year	0.5°S, 78.04°W	2,950 m	X	X	Baker et al. (2022)
Pumacocha	Laguna Pumacocha	Lake sediment	1 year	10.70°S, 76.06°W	4,300 m	X		Bird et al. (2011)
Bol	Purisima, Selva Negra	Cedrela odorata tree-ring cellulose	1 year	11.0°S, 66.92°W	160 m	X	X	Baker et al. (2022)
P00-HI	Huagapo Cave	Speleothem	5 years	11.27°S, 75.79°W	3,850 m	X		Kanner et al. (2013)
PIM4	Cuica Cave	Speleothem	1 year	11.67°S, 60.63°W	310 m	X		Della Libera et al. (2022)
DV2+TR5+LD12	Diva Cave	Speleothem	1 year	12.36°S, 41.57°W	700 m	X		Novello et al. (2012)
SBE3	São Bernardo, São Matheus Caves	Speleothem	0.2 years	13.81°S, 46.35°W	631 m	X		Moquet et al. (2016), Novello et al. (2018)
Quelccaya	Quelccaya Ice Cap	Ice core	1 year	13.93°S, 70.83°W	5,670 m	X	X	Thompson et al. (2013)
JAR4	Jaraguá Cave	Speleothem	5.5 years	21.08°S, 55.58°W	570 m	X		Novello et al. (2018)
UTU	Uturuncu Volcano	Polylepis tarapacana tree-ring cellulose	1 year	21.7°S, 66.77°W	4,457 m	X	X	Rodriguez-Catón et al. (2024)
CR1	Cristal Cave	Speleothem	4 years	24.66°S, 49.54°W	130 m	X		Vuille et al. (2012)
MFZ-N-1	Malfazido Cave	Speleothem	0.5 years	24.58°S, 48.58°W	885 m	X	X	Cauhy Rodrigues, et al. (2022)

Note. Sampling resolution is given for the period of study for each record (1880–2000 CE). For each record, an ‘X’ in the IPO and/or ENSO column indicates that record was used for the mode analysis.

paleoclimate records in time by a few years, would likely retain the same IPO phase signal. A case study from central Brazil showed that correlations between speleothem $\delta^{18}\text{O}_p$ and local precipitation is maximized when precipitation is smoothed with a 7–9 years filter (Moquet et al., 2016), highlighting the potential utility of speleothem records for decadal or multidecadal signal detection. For speleothem records in the IPO interpretation network, with the exception of the MFZ-N-1 record, we applied a Monte Carlo resampling of the dating uncertainty of published records to preserve age model uncertainty in the $\delta^{18}\text{O}_p$ timeseries and utilized the median time series for analysis in this study. These timeseries were subsequently annually interpolated to match the remaining records, but are limited to multidecadal interpretation as a result. Further details of this method are discussed in Orrison et al. (2022).

Precipitation-weighted oxygen isotope data from the IAEA-GNIP database (IAEA/WMO, 2023) were also used to validate the model simulations of $\delta^{18}\text{O}_p$ and compared with terrestrial proxy data in the composite analysis. These data are part of a worldwide observational network, maintained by the IAEA under the umbrella of the World Meteorological Organization (WMO). Data is temporally and spatially sparse—some station records date from 1960, but are often discontinuous and range in length from 1 year to several decades. Therefore, care has been taken in selecting and interpreting these records. Data were extracted from stations that met two criteria: (a) only those stations with more than seven seasons of available data were used, where a season was defined as containing at least 2 months of available data from DJF; and (b) all stations were required to have at least 3 years of data in both a positive and negative phase of the IPO (Figures 2a and 2b). The isotopic signature of austral summer (DJF) precipitation was calculated using precipitation-weighted seasonal averages of available data. Anomalies were calculated on a station-by-station basis for available data relative to a common base period of 1965–1985 CE. Outlier values exceeding two standard deviations from the mean were excluded from the analysis.

Monthly precipitation data based on observations from the Global Precipitation Climatology Center (GPCC) gridded data set (0.5° resolution) were used to calculate correlations between IPO and ENSO and precipitation time series derived from locations of terrestrial $\delta^{18}\text{O}$ records from paleoclimate archives and IAEA stations (Schneider et al., 2011). GPCC data were seasonally averaged for austral summer (DJF) from 1890–2000 CE.

3.3. Correlation and Regression Analysis

Analysis of the hydroclimate response was performed based on compositing, correlation, and regression analysis. Compositing analysis considers a non-linear response of the hydroclimate to Pacific Ocean modes, performed by calculating the difference between temporal averages of the positive and negative phase years of the IPO and ENSO. Correlation and regression analyses, on the other hand, presume a linear response of South American $\delta^{18}\text{O}$ to both phases of the ENSO and IPO. Correlation and regression fields between the IPO and hydroclimate were calculated by linearly detrending data and applying an 11-year smoothing to modeled hydroclimate parameter timeseries (oxygen isotopes in precipitation ($\delta^{18}\text{O}_p$), precipitation (P), 500 hPa vertical velocity (ω_{500}), 200 hPa geopotential height (Z200) and 200 hPa horizontal winds (u200,v200)) to conform with the smoothing applied to the IPO timeseries, following He et al. (2021). Terrestrial archives without signal mixing between layers (Lake Pumacocha, tree-ring cellulose archives) were also smoothed with an 11-year running mean to isolate the low-frequency signal.

Local statistical significance of the difference between the two phase composites of each mode and the Pearson correlation analysis was calculated using a Student's *t*-test with a significance level of $p \leq 0.05$. For the IPO, the smoothing filter applied to the TPI and model parameters functions as a low-pass filter. An effective degrees of freedom ($\text{DOF}_{\text{eff}} = 26.67$) was calculated to account for the loss of sample independence from this filtering and the DOF_{eff} was used to calculate a modified *t*-statistic and *p*-value evaluating the statistical significance of the correlations. The DOF_{eff} was calculated as $\text{DOF}_{\text{eff}} = 2 * L / \text{LPP} - 2$, where L is the length of the full period of study ($L = 120$) and LPP is the low-pass filter period (LPP = 11), following Steinman et al. (2022).

The large-scale atmospheric circulation response to Pacific SST forcing using iCAM5 simulations was approached from a local, continental, and regional view. First, running correlations between mid-tropospheric vertical motion (ω_{500}) in the entrance region of the monsoon (5°S–10°N, 65°W–40°W) and $\delta^{18}\text{O}_p$ in the monsoon core (15°S–0°S, 75°W–60°W) and between precipitation (P) and $\delta^{18}\text{O}_p$ in the monsoon core (see dashed black boxes in Figure 4) were calculated to evaluate the relative importance of upstream convection versus local rainout for the monsoon (DJF) isotopic signal. Additionally, the running correlation between N3.4 and monsoon core $\delta^{18}\text{O}_p$ was calculated to evaluate the stationarity of the ENSO— $\delta^{18}\text{O}_p$ relationship in time over this region.

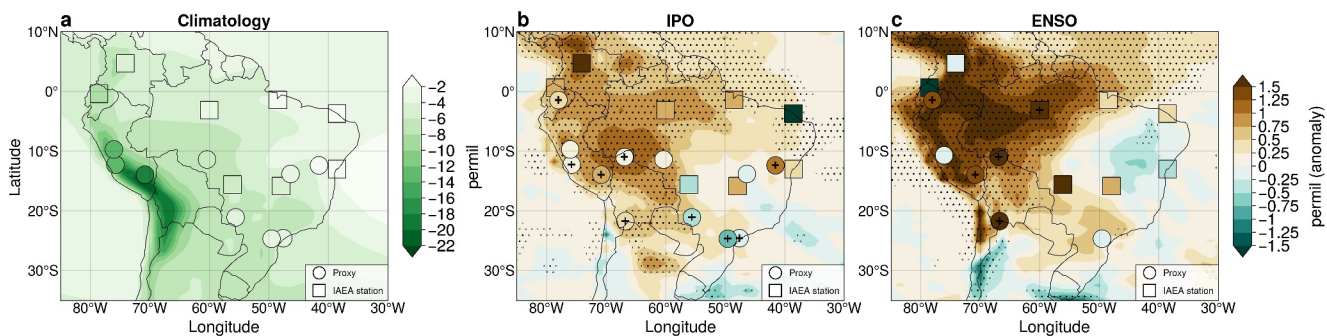


Figure 3. SASM (DJF) $\delta^{18}\text{O}_p$ climatology and its response to Pacific Ocean modes. $\delta^{18}\text{O}_p$ data are from the iCAM5 model (shading), terrestrial proxy records (circles), and IAEA station observations (squares). (a) DJF precipitation-weighted average of $\delta^{18}\text{O}_p$ (1880–1999 CE). Composites of positive–negative phase years for (b) IPO and (c) ENSO. Reference period for iCAM5 and proxy data cover the full study period of 1880–1999 CE and IAEA data are available from 1965–1986 CE. Statistical significance at $p < 0.05$ is indicated with a black cross for proxy records and IAEA stations and with black stippling for model simulations. Pumacocha, P00-H1 and CR1 records are shifted slightly for visibility.

The correlation timeseries were smoothed with a 31-year running average to highlight the influence of positive and negative phases of the IPO on the strength of these correlations. Second, changes in the Walker circulation (zonal tropical circulation) were diagnosed along a longitudinal cross-section (100°W – 10°W), over equatorial South America (averaged over 5°S – 10°N), including the entrance region of the SASM onshore flow, using oxygen isotopes in water vapor ($\delta^{18}\text{O}_v$), specific humidity (q), and meridionally averaged zonal winds (u) and vertical motion (ω) in the iCAM5 model. Finally, the upper-level (200 hPa) horizontal wind field (u_{200} , v_{200}) and geopotential height (Z_{200}) were regressed against the TPI and N3.4 to highlight the pathways of atmospheric reorganization by which the Pacific SST forcing affects large-scale circulation and modulates hydroclimate over tropical South America.

4. Results

4.1. Observed and Simulated South American Hydroclimate Response to Pacific SST Variability

Composites of the positive minus negative phase years of Pacific SST modes show distinct and statistically significant differences in their $\delta^{18}\text{O}_p$ anomaly fields (Figure 3). The $\delta^{18}\text{O}_p$ climatology across the continent is characterized by a relatively weak continental gradient featuring only slightly negative values along the coast and increasingly more negative values inland, with the strongest depletion of heavy isotopes occurring in areas of strong orographic uplift downstream of the core monsoon region over the Central Andes. The model, raw proxy records, and IAEA station observations all agree on the nature of this continental effect (Vuille, Bradley, Werner, et al., 2003) (Figure 3a). Tree-ring $\delta^{18}\text{O}$ records were excluded from the climatology in Figure 3a due to the enrichment of $\delta^{18}\text{O}$ values by biological processes during cellulose formation at leaf level via the mixing of leaf sugars and xylem water, which carries the imprint of the source water signal ($\delta^{18}\text{O}_p$) (McCarroll & Loader, 2004).

Composite difference plots show the magnitude and extent of the $\delta^{18}\text{O}$ response across tropical South America that can be expected during the Pacific positive and negative phase based on model, proxy, and observational evidence (Figures 3b and 3c). Despite the unique character of each data type, a first-order, linear interpretation shows that there is a continent-wide response of isotopes to the extreme phases of the Pacific modes. Positive values indicate regions where the positive phase results in an enrichment of heavy isotopes in precipitation, and a stronger depletion of heavy isotopes occurs during the negative phase. Indeed, positive and negative phase composites show similar, though inverse, $\delta^{18}\text{O}_p$ response patterns (not shown). The regions within tropical South America that show the greatest isotopic differences between the two phases are the western Amazon basin and the tropical Andes. In the case of the model simulation of the $\delta^{18}\text{O}_p$ response to IPO, this influence extends into northern Argentina (Figure 3b). Paleoclimate records and IAEA stations within the tropical and central Andes tend to show slightly more negative $\delta^{18}\text{O}_p$ anomalies compared to the model simulations, likely due to an underestimation of depletion in heavy isotopes due to reduced orographic rainout associated with the muted model topography.

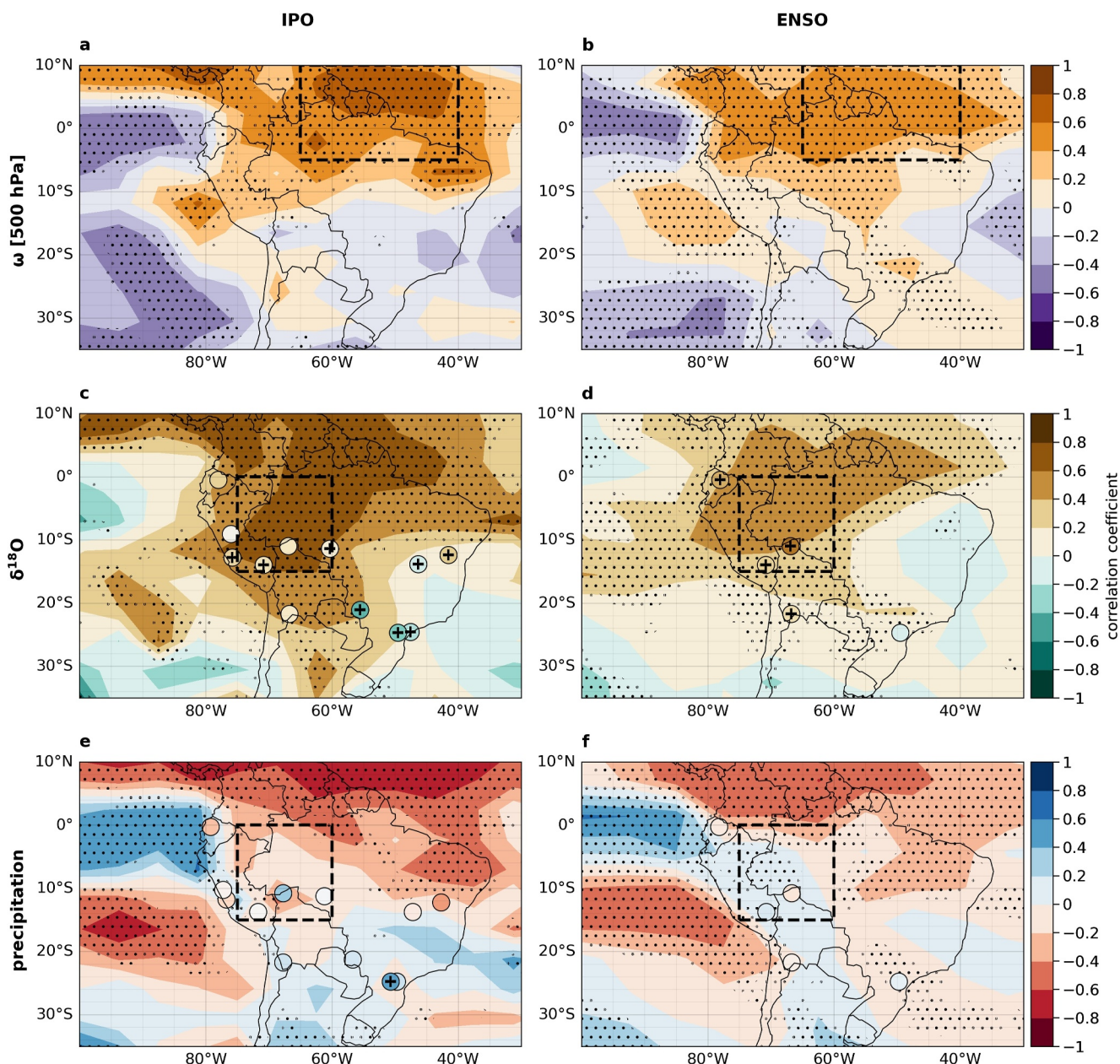


Figure 4. Correlations between Pacific SST modes and South American DJF hydroclimate, including (a) IPO and ω_{500} hPa from iCAM5, (c) IPO and $\delta^{18}\text{O}_p$ from iCAM5 and proxy records (plotted as circles), (e) IPO and precipitation from iCAM5 and GPCC (plotted as circles); (b, d, and f) as in (a, c, and e) but for ENSO. The core region of the ω_{500} and $\delta^{18}\text{O}_p$ responses to ENSO and IPO indices are outlined in dashed boxes. Statistical significance at $p < 0.05$ is indicated with a black cross (proxies) and black stippling (model).

There is a stronger isotopic response to ENSO than to the IPO on average, and the core ENSO response is located to the north of the IPO response. The iCAM5 model, proxy records and IAEA observations generally agree on the sign of the response throughout the monsoon domain and show anomalies that are of comparable magnitude. The IAEA observations display less statistical confidence due to, in part, the limited temporal availability. Additionally, a few stations in the network report results that are markedly different than nearby proxy records or the background model results. Of particular note is the ENSO signal at the Izobamba IAEA station, where the negative $\delta^{18}\text{O}$ anomaly contrasts with the positive anomalies seen in the model and proxy data nearby. While this result highlights the importance of understanding data availability, these IAEA stations nevertheless provide invaluable information in locations where proxy and model data disagree. For example, the IAEA Cuiabá station

agrees with the proxy results in the SESA region (JAR, MFZ-N-1, CR1), capturing a negative response to the IPO phase difference—a signal which is not captured by the modeled $\delta^{18}\text{O}_p$ in iCAM5 (Figure 3b).

Overall, these results support the use of proxy records for documenting hydroclimate responses to both IPO and ENSO modes in the past across tropical South America as well as in the present day, as validated by IAEA data. Given the statistical significance of the IPO differences seen in many of the proxy records across South America, evidence strongly suggests that the IPO is an important mode of internal variability that can influence $\delta^{18}\text{O}$ records across South America during the monsoon season, though the development of longer and more paleoclimate records would help to clarify regional discrepancies arising from both model and observational data.

Correlation maps of ENSO and IPO indices with ω_{500} , $\delta^{18}\text{O}_p$, and precipitation based on iCAM5 simulations further illustrate the coupling of the Pacific modes to South American isotope hydroclimate. These relationships document broad, spatially coherent, and statistically significant links between Pacific SST anomalies and hydroclimatic variability over South America (Figure 4). The smoothing of both the TPI timeseries and model-derived hydroclimate fields isolates the low-frequency climate response, resulting in stronger IPO correlations relative to the ENSO correlation values. However, the stronger IPO correlations should be interpreted in the context of reduced degrees of freedom due to the smoothing and hence should not be interpreted as a more significant climate response to the low-frequency Pacific forcing. Indeed, Figure 3c shows that the South American hydroclimate response to ENSO is stronger than that due to IPO forcing. Regions of South America that are most strongly associated with key monsoon processes (indicated by black boxes in Figure 4) show notable coupling to the Pacific, which are similar for both low- and high-frequency modes.

Strong positive correlations exist between the Pacific indices and the ω_{500} field over the monsoon entrance region (black boxes in Figures 4a and 4b), where onshore flow transports tropical North Atlantic moisture toward the continent via trade wind convergence and the land-sea pressure gradient. The positive correlations indicate that anomalously warm (cool) Pacific SSTs result in reduced (increased) upward motion across the tropical Atlantic, the Guianas, and the northern Amazon. Weaker convection in this region linked to warm Pacific SSTs has consequences for the downstream water cycle, recorded by both oxygen isotopes and precipitation.

The stable oxygen isotopes in the core of the monsoon region (black boxes, Figures 4c and 4d) are positively correlated with the Pacific modes, implying that rainfall during the positive SST phases is more enriched in heavy isotopes. The convective processes upstream modify the isotopic composition of the source moisture, which then converges over the continent and is steered southwestward by low-level winds into the monsoon core domain. Proxy records in this region agree with the sign of the model correlations, with several of them recording a significant ENSO and IPO signal, albeit with a weaker correlation relative to that between modeled isotopic values and Pacific mode indices (Figures 4c and 4d). This is, in part, potentially attributable to the low-frequency filter applied to the iCAM5 data and will require further exploration.

Model simulations of precipitation in the monsoon core region (black boxes, Figures 4e and 4f) show little coherence and weak statistical significance in their response to the Pacific modes across the Amazon basin, highlighting the importance of comparing paleoclimate records directly with isotope-enabled simulations to diagnose the large-scale influence of Pacific modes of variability. However, correlations between Pacific modes and GPCC precipitation data at terrestrial $\delta^{18}\text{O}_p$ archive locations show significant negative values at those locations where positive $\delta^{18}\text{O}_p$ correlations are recorded. In the model, the region with the strongest correlation between precipitation and Pacific modes exhibits positive values and is located over tropical South America north of the equator in regions not typically associated with monsoon rainfall (Colombia and Venezuela), the Guianas, and northeastern Brazil, consistent with correlations between these modes and the gridded precipitation data (Figure S1 in Supporting Information S1). The model precipitation response over the monsoon core is muted in response to high- and low-frequency modes compared to the precipitation response in the upstream domain, while stable oxygen isotopes in the core region more strongly reflect a signal of Pacific variability. This highlights the added value of using isotope-enabled climate models in combination with proxy records when interpreting hydroclimate variability as recorded in stable isotopic records.

In addition to the tropical monsoon response, model simulations highlight another important area of coupling between Pacific SST variability and South American convection to the south of the climatological position of the SACZ (see Figure 2). Significant positive correlations are apparent between the N3.4 index and ω_{500} along the continental and oceanic SACZ region of southeastern Brazil, indicating decreased (enhanced) convection during

the Pacific positive (negative) phase. The anomalous subsidence in this region implied from the model results during the El Niño phase of ENSO is physically consistent with the correlations between the indices and the simulated hydroclimate response in the SACZ region: anomalously warm SSTAs lead to positive $\delta^{18}\text{O}_p$ anomalies while the regional rainfall amount is reduced. However, particularly in response to the IPO, paleoclimate results and GPCC data disagree with these simulated dynamics. While the iCAM5 simulations do not show a strong response to the IPO in this region, paleoclimate records reflect a statistically significant negative relationship with the low-frequency signal. Figures 4c and 4d show negative correlations between IPO/ENSO and $\delta^{18}\text{O}_p$ in paleoclimate records in the SACZ region, indicating warm Pacific SSTA correspond to negative $\delta^{18}\text{O}_p$ anomalies—a response opposite to that recorded by upstream terrestrial $\delta^{18}\text{O}_p$ archives. Despite model simulations showing a uniform regional response to the Pacific forcing across much of tropical and sub-tropical South America, the archives from southeastern Brazil paint a different picture. The negative correlations between the Pacific indices and paleoclimate records reflects a regional signal of mixed fractionation processes that integrate, at a minimum, both the upstream monsoon signal with a local precipitation signal. This has previously been noted at multi-centennial timescales from the Botuverá Cave (Cruz et al., 2005). The GPCC data from this region show significant positive correlations with the IPO, indicating an increase in precipitation in response to warm Pacific SSTA. This positive local rainfall response to warm Pacific SSTA has been previously documented during positive IPO and ENSO periods (Flantua et al., 2016; Marengo & Espinoza, 2016). These results support a locally anomalous “amount effect” footprint over southeastern Brazil in response to the warm phase of the Pacific modes, which is not captured by iCAM5 simulations.

Proxy evidence for this local hydroclimate response is consistent with research on synoptic timescales that finds increased baroclinicity during the ENSO/IPO positive phases induce more rainfall linked to increased moisture convergence and Rossby waves emanating from the tropical Pacific enhancing the subtropical jet (Garreaud et al., 2009; Grimm, 2003). However, further research is needed to better understand the disconnect between the observed regional isotopic signal and the hydroclimate/dynamic mechanisms leading to the divergent response simulated by iCAM5.

Other regions in South America less directly associated with the monsoon are also impacted by high- and low-frequency modes of Pacific variability. Along the coast of South America over Ecuador and Peru, a dipole of negative/positive correlations between IPO/ENSO and ω_{500} can be seen. The positive correlation between ENSO and ω_{500} is broader relative to that between IPO and ω_{500} over the tropical Andes and central Peru. Correlations between oxygen isotopes and the Pacific modes are generally positive (indicating ^{18}O enrichment in the positive phase) across tropical South America, the northern and central Andes mountains, and extending south into Bolivia, Paraguay, northern Argentina, and southeastern Brazil. This response is spatially more uniform than the correlations with precipitation in the model simulations.

4.2. Regional Hydroclimate and $\delta^{18}\text{O}$ Dynamics

Correlations between hydroclimate variables averaged over IPO- and ENSO-sensitive regions in South America reveal further insight into the physical mechanisms that impact the $\delta^{18}\text{O}_p$ in the core of the monsoon domain within the context of the iCAM5 simulations. The spatially averaged timeseries of $\delta^{18}\text{O}_p$ from the monsoon core (black box in Figures 4c and 4d) was correlated against the spatially averaged timeseries of ω_{500} in the entrance region (black box in Figures 4a and 4b) and precipitation in the monsoon core (black box in Figures 4e and 4f). Running correlations among these timeseries based on a 31-year running mean show a strong relationship between $\delta^{18}\text{O}_p$ and upstream vertical motion throughout the period of study (Figure 5, orange line). The local precipitation amounts are not as strongly linked to the temporal evolution of the monsoon core $\delta^{18}\text{O}_p$ timeseries and show the most significant correlation during the IPO warm phases (Figure 5, green line). Notably, the correlation of entrance region convection with monsoon core $\delta^{18}\text{O}_p$ appears to be largely unaffected by the change of the IPO phase (Figure 5, vertical red/blue bars). The critical role of upstream vertical motion in modulating downstream $\delta^{18}\text{O}_p$ is stable throughout the study period and likely due to the fundamental control of upstream convective activity on the isotopic composition of monsoon precipitation within this core region. The upstream control is measured by the strength of vertical velocity at 500 hPa, representing an approximation of the various convective processes at play which merit further decomposition and investigation. While the co-variability of ω_{500} and $\delta^{18}\text{O}_p$ is shown here to be tightly coupled as a constant of SASM dynamics, the large-scale drivers of this mechanism might vary in time.

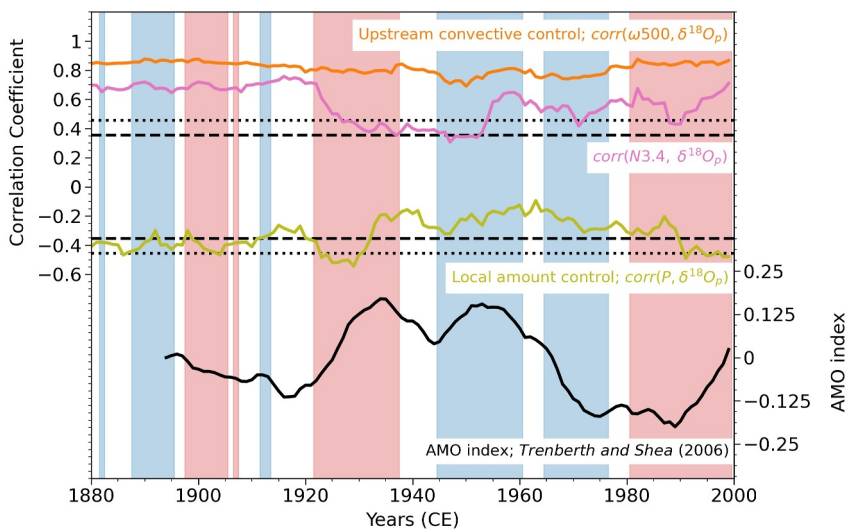


Figure 5. Temporal evolution of physical processes driving $\delta^{18}\text{O}_p$ in SASM core region. Correlations between 31-year running averages of area-averaged timeseries derived from boxes shown in Figure 4 as simulated by iCAM5. Correlation between ω_{500} and $\delta^{18}\text{O}_p$ (orange line) represents the strength of upstream convective control on downstream $\delta^{18}\text{O}_p$. Correlation between $\delta^{18}\text{O}_p$ and P (green line) indicates local precipitation control on oxygen isotopes (“amount effect”). The pink line shows the correlation between the N3.4 index and $\delta^{18}\text{O}_p$. The black line is the AMO index (Trenberth & Shea, 2006). Red and blue shading highlight positive and negative phases of the IPO, respectively. All variables reflect the DJF averaged values. Confidence levels based on the adjusted degrees of freedom ($df = 29$) for 31-year smoothed timeseries are indicated for the 95%-significance level (dashed lines) and 99%-significance level (dotted lines).

The running mean correlation between the N3.4 timeseries and the $\delta^{18}\text{O}_p$ from the core of the monsoon region is mostly significant and positive (Figure 5, pink line). This indicates an important role for ENSO dynamics in controlling $\delta^{18}\text{O}_p$ variability in the monsoon core, potentially via the upstream pathway. Interestingly, the correlation of the ENSO index with the monsoon core $\delta^{18}\text{O}_p$ record is relatively agnostic of the IPO phase (Figure 5, red/blue shading). Thus, while the IPO does have a role to play in terms of influencing monsoon variability, it does not do so via modulation of the ENSO impact, but rather as a distinct forcing.

However, the correlation between the N3.4 time series and the iCAM5 simulations of monsoon core $\delta^{18}\text{O}_p$ weaken from around 1925 to 1955 CE, indicating a decoupling of this otherwise stable relationship. Interestingly, the AMO enters a positive phase during this period of decoupling. A Student's *t*-test confirms that the N3.4- $\delta^{18}\text{O}_p$ correlation values during the positive and negative AMO phases are statistically highly distinct from one another ($p < 0.001$). The AMO has also been noted as a historical driver of $\delta^{18}\text{O}_p$ variability in paleoclimate archives across the monsoon basin (Apaéstegui et al., 2014), indicating the importance of continued study of inter-basin interactions to fully understand the implications for isotope variability within the SASM domain.

4.3. Monsoon Dynamic Response to Pacific Modes of Variability

The mean state of the peak monsoon season (Figures 6a and 6d), as simulated by iCAM5, shows strong onshore flow from the tropical North Atlantic in the lower troposphere below 850 hPa and upward motion throughout the atmospheric column above the continent. The background $\delta^{18}\text{O}_v$ and specific humidity fields illustrate the depletion of heavy isotopes and drying of the atmosphere with height. Difference plots between the composited extreme mean states of the positive and negative phases of the IPO (Figures 6b and 6c) and ENSO (Figures 6c and 6f) show the anomalies of circulation and vapor that develop over the monsoon entrance region in response to Pacific SST anomalies.

The difference between the two phases of both IPO and ENSO reinforces the first-order response of weakened (strengthened) monsoon convection in the total atmospheric column above South America during the positive (negative) phase extremes, with the positive phase response dominating the difference field (not shown). The difference between the two IPO phases is most significant in vertical motion of the mid- and upper troposphere while the lower levels of the atmosphere exhibit a weaker dynamic response that implies a local reduction in

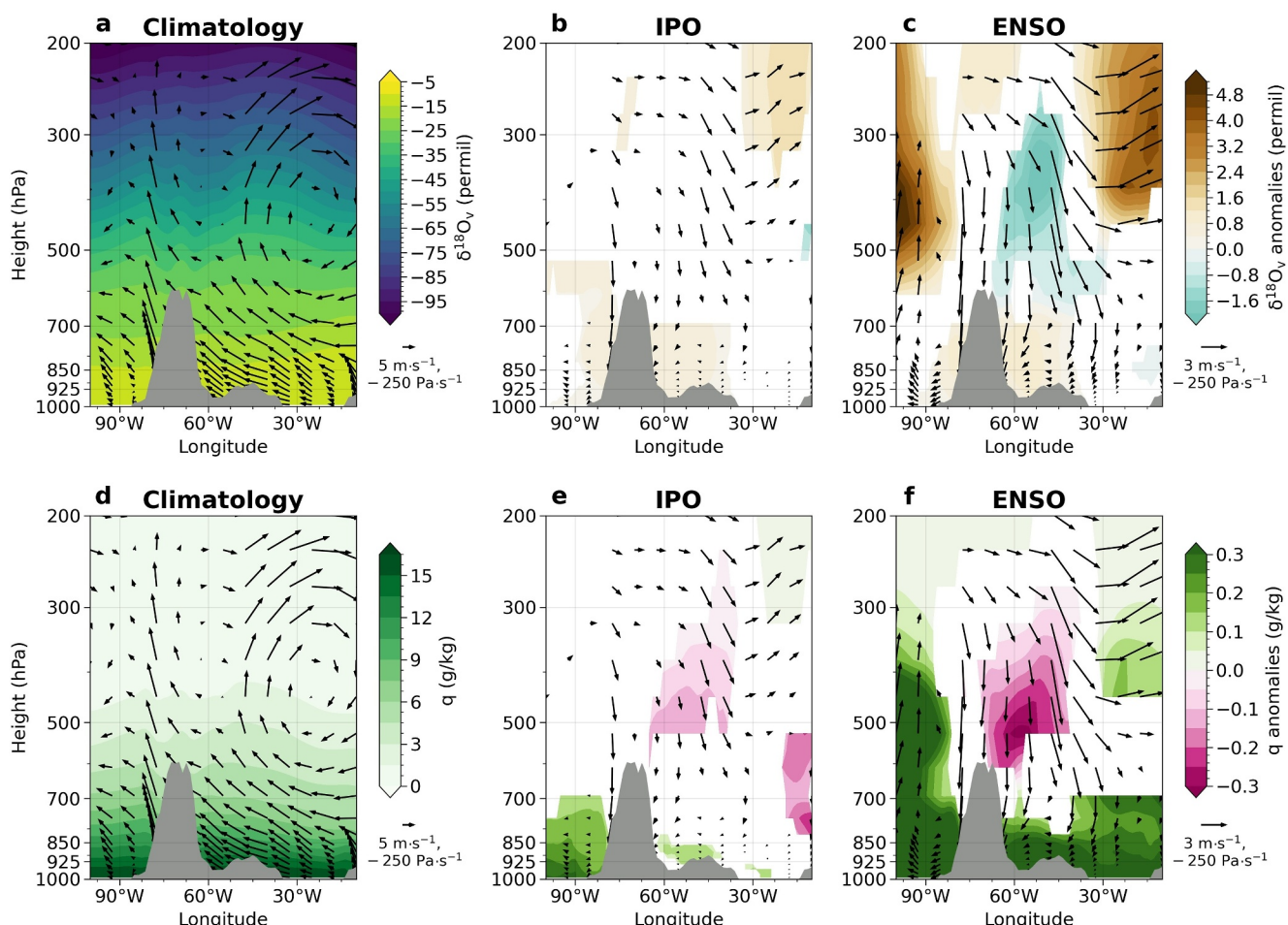


Figure 6. Longitudinal cross-sections of the regional Walker circulation (zonal wind and vertical motion) averaged between 5°S and 10°N and oxygen isotopes of water vapor ($\delta^{18}\text{O}_v$) as simulated by iCAM5 during DJF. (a) Seasonal climatology for period of study (DJF; 1880–2000 CE), (b and c) difference between the positive minus negative phase composites of the (b) IPO and (c) ENSO modes. (d–f) are the same as (a–c) but showing specific humidity (q). The cross-section spans the eastern Pacific, South America (maximum model topography illustrated with gray shading), and western Atlantic. In (b and c) and (e and f) only statistically significant vectors (either u or ω , or both) and color shading are plotted ($p < 0.05$).

convection (Figure 6b). The dynamic differences between the ENSO phases are consistent with the IPO pattern, though with an overall stronger response that shows reduced mid-tropospheric convergence and anomalous downward vertical motion in the lower troposphere (Figure 6c).

Thermodynamic changes associated with the differences between convective activity during the positive and negative Pacific phases alter the vapor field and isotopic composition of water vapor in the atmosphere. Differences of $\delta^{18}\text{O}_v$ between the two IPO phases show enrichment in heavy isotopes and are significant in the lower troposphere only (below 700 hPa, Figure 6b), while specific humidity differences show drying in the mid-troposphere and increased specific humidity in the lower troposphere (Figure 6e). Differences between the ENSO phases show significant $\delta^{18}\text{O}_v$ anomalies throughout the atmospheric column (Figure 6c) and consistent specific humidity changes (Figure 6f). Lower tropospheric $\delta^{18}\text{O}_v$ and q differences are consistent with those in the difference between IPO phases, showing enriched $\delta^{18}\text{O}_v$ and increased specific humidity. In the mid-troposphere (above 700 hPa), negative $\delta^{18}\text{O}_v$ anomalies and corresponding atmospheric aridity during the ENSO positive phase are coincident with the anomalous reduction of convection, with the inverse signals seen during the ENSO negative phase.

Convective processes contribute to a vertical $\delta^{18}\text{O}_v$ dipole between lower and middle troposphere, albeit significant only in the case of ENSO (Figure 6c). This dipole simulated by iCAM is consistent with observations from thermal infrared remote sounding observations which show that the isotopic composition of water vapor in

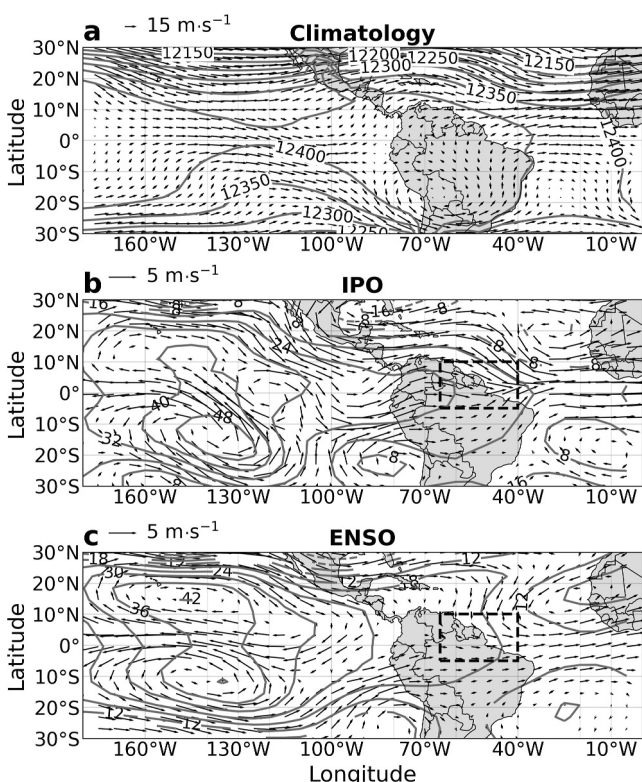


Figure 7. Simulated DJF 200 hPa horizontal winds (vectors) and geopotential height (contours) from iCAM5 plotted as (a) climatology (1880–2000 CE) and regressed against (b) IPO and (c) the ENSO. Contour interval for z -values is (a) 50 m and (b and c) 8 m per unit std. dev., respectively. Scaling vectors for wind field are shown above each plot. The core region of the Walker circulation (via ω_{500}) response to ENSO and IPO indices is outlined as a dashed box in (b, c).

ric about the equator at approximately 10°S and 10°N, ~140°W (Sulca et al., 2018; Vuille, Bradley, Healy, et al., 2003). Rossby waves initiated by diabatic heating can be seen propagating away from these anticyclones and the anomalous upper-level westerly flow follows geopotential heights downstream over tropical South America and the Caribbean (Andreoli & Kayano, 2005). Ultimately, the anomalous flow converges over the equatorial Atlantic and northern Brazil (black dashed box), effectively suppressing convective activity over this region during the IPO/ENSO positive phase. Indeed, this is the same region that shows a strong correlation between 500 hPa vertical motion and ENSO/IPO (same box as shown in Figures 4a and 4b), where 500 hPa vertical motion is strongly correlated with western Amazon $\delta^{18}\text{O}_\text{p}$ variability as seen in Figure 5, and the South American sector of Walker circulation anomalies are strongly perturbed during IPO/ENSO (Figure 6). To the south of the monsoon core, an anomalous cyclone is formed in response to both the IPO and ENSO positive phase, indicating a weakening of the Bolivian High and shift of this feature to the southwest of its climatological position. This shift has been previously observed, and, coupled with anomalous upper-level westerlies, identified as a mechanism that inhibits the transport of depleted $\delta^{18}\text{O}_\text{v}$ toward the north-central Andes (Insel et al., 2013). The atmospheric pathway by which the IPO exerts control on SASM isotopic variability thus mirrors the mechanism by which ENSO controls South American isotopic hydroclimate (e.g., Vuille & Werner, 2005).

5. Discussion

The IPO and ENSO forcing of SASM isotopic variability is apparent in the iCAM5 model results, the paleoclimate records, and in GNIP data. The compositing of positive minus negative phases of the IPO and ENSO leads to results that are consistent between model simulations, paleoclimate archives, and GNIP data. Field correlations between Pacific modes and the paleoclimate records and the iCAM5 model simulations document the importance of both interannual and multidecadal Pacific SST anomalies in modulating monsoon hydroclimate, and reinforce

the mid-troposphere (~4.5 km) is quite sensitive to the intensity of convection and that the convective depth determines the altitudes at which convection depletes or enriches its environment (Galewsky et al., 2016; Lacour et al., 2018). Additional mechanisms associated with changes in convective intensity likely influence this vertical dipole of $q - \delta^{18}\text{O}_\text{v}$ anomalies, such as the entrainment of middle and upper tropospheric air into the lower atmosphere that correlates with strong convection (Moore et al., 2014), and condensation processes (Samuels-Crow et al., 2014). Changes in the local Walker circulation branch during the positive (negative) phases of Pacific modes could significantly reduce (enhance) the vertical mixing within the atmospheric column and entrainment of the surrounding atmosphere, thereby affecting the strength of various fractionation processes.

Changes in the Walker circulation resulting from Pacific internal variability are further illustrated from the perspective of the upper-level (200 hPa) circulation. The DJF mean wind field and geopotential height illustrate the climatological westerly flow which forms part of the upper branch of the Walker circulation over the central tropical Pacific (Figure 7a). The upper level winds branch to the north and south of the tropical Andes in geostrophic balance with geopotential height. To the south, the tropical jet follows the wave guide of the Bolivian High–Nordeste Low system, formed as a result of the convection and latent heat release over the Amazon Basin (Chen et al., 1999; Lenters & Cook, 1997). The presence of the Bolivian High–Nordeste Low system is noted here with anticyclonic flow to the southwest of the Amazon and an upper-level trough off the coast of eastern Brazil (Figure 7a).

The regression of these fields against the IPO/ENSO indices shows how the monsoon climate responds to heating anomalies in the equatorial Pacific (Figures 7b and 7c), mapping the upper level response to a unit change of the Pacific index. The latent heat released as a result of convective activity over the tropical Pacific during the ENSO/IPO positive phase drives upper-level equatorial divergence, forming two anomalous twin anticyclones, symmetric

the link between upstream convective activity and Amazon basin $\delta^{18}\text{O}_p$ (Orrison et al., 2022). These results are consistent with the conclusions of Midhun et al. (2021) but show a more robust agreement between paleoclimate records and the iCAM5 simulations relative to the fully coupled simulations over South America, highlighting the known difficulty for coupled models to accurately simulate internal modes of climate variability (Fasullo et al., 2020).

The iCAM5 model simulations simulate well the spatial coherency of $\delta^{18}\text{O}_p$ across tropical and subtropical South America in alignment with paleoclimate records. Though the precipitation response shows a weaker coupling to the IPO and ENSO modes in the iCAM5 model simulations, the internal dynamic coupling of the monsoon core $\delta^{18}\text{O}_p$ with upstream vertical velocity is well reproduced. The variability of $\delta^{18}\text{O}_p$ during the mature monsoon season is modulated by Pacific modes of SST variability via changes in monsoon dynamics, particularly the convection over the monsoon entrance region (Figure 4).

The reorganization of the large-scale zonally overturning circulation in the tropical Pacific—South America sector is apparent in the anomalous regional Walker circulation and results in enhanced or suppressed convection over the tropical North Atlantic (Figure 6), a region which has previously been noted as tied to monsoon intensity and control of $\delta^{18}\text{O}_p$ in the Andes (Atwood et al., 2021; Fiorella et al., 2015; Orrison et al., 2022; Vuille & Werner, 2005). The Pacific Walker circulation reorganization in response to IPO phase shifts has also been identified as driving oxygen isotope variability over the Maritime Continent and northern Australia (Falster et al., 2021). The structure of the tropospheric $\delta^{18}\text{O}_v$ response to ENSO and IPO forcing over tropical South America provides mechanistic insight into how the South American Summer monsoon convection is being modulated by the two Pacific modes. The height and intensity of the convection in the troposphere controls the partitioning between positive and negative $\delta^{18}\text{O}_v$ anomalies seen in the vertical dipole (Figure 6). The reduction of deep convection during Pacific positive phases, such as is present in the monsoon entrance region, is associated with a variety of possible fractionation mechanisms which can influence the background $\delta^{18}\text{O}_v$ and specific humidity fields (Galewsky et al., 2016). The depletion of heavy isotopes in water vapor seen in the mid- and upper troposphere is consistent with remote sensing observations (Lacour et al., 2018) and model simulations of Walker circulation change over the Pacific (Dee et al., 2018). In the lower-troposphere below the cloud layer, reduced convection produces less precipitation which could potentially increase the evaporation from falling rain, resulting in more enriched $\delta^{18}\text{O}_v$ and greater specific humidity near the surface (Lacour et al., 2018; Risi et al., 2008). Additionally, Moore et al. (2014) suggest another possible mechanism coupled to convective intensity changes, whereby weakened convective strength reduces downward vertical entrainment of middle and upper troposphere specific humidity and $\delta^{18}\text{O}_v$ anomalies into the lower troposphere, possibly reinforcing the isotopic vapor-precipitation balance driven by convection and rainout. Reduced vertical motion could also inhibit the lofting of lower-tropospheric vapor upward from the surface, trapping greater specific humidity and $\delta^{18}\text{O}_v$ enriched in heavy isotopes near the surface. While the above mechanisms are suggested as central to the $\delta^{18}\text{O}_v$ and specific humidity anomalies identified here in response to the perturbation of the Walker circulation, other mechanisms affecting isotopic fractionation during phase changes between water vapor and precipitation could be relevant to the $\delta^{18}\text{O}_p$ variability captured by terrestrial archives and model simulations, including changes in evaporation rates and source, vapor saturation and condensation temperature changes, meso-scale air mass exchange, and post-condensational processes (Fiorella et al., 2021; Galewsky et al., 2016). Further diagnosis to weigh the contributions from discrete fractionation mechanisms influencing the $\delta^{18}\text{O}_v$ in the monsoon entrance region and preconditioning the downstream $\delta^{18}\text{O}_p$ signal is an important next step that should follow from these initial results.

Stable oxygen isotopes in South America have been known to record ENSO variability. This has been evaluated in climate models and ice cores, documenting the relative importance of different climate variables such as source region, temperature change, and precipitation amount change in response to interannual Pacific SST variability (Bradley et al., 2003; Hurley et al., 2019; Vuille, Bradley, Werner, et al., 2003). The high-frequency signal of El Niño events has been linked to anomalously positive $\delta^{18}\text{O}$ values in a number of proxy records across the monsoon basin (Baker et al., 2022; Rodriguez-Caton et al., 2022; Thompson et al., 2013) and negative values in southeastern Brazil (Cauhy Rodrigues et al., 2022). Past studies using isotope-enabled models and isotopic forward models have documented the ENSO influence on the SASM and illustrated the decoupling of the isotopic composition from local precipitation amount and instead emphasized the importance of upstream convective activity and circulation changes; yet these studies have been limited to short periods (Hurley et al., 2019; Vuille & Werner, 2005). Here we use a much longer, 120-year period to statistically link oxygen isotope variability in

paleorecords, including novel, annually resolved records from tree-ring cellulose and carbonate speleothems, and a state-of-the-art isotope-enabled atmospheric model with prescribed SST. ENSO-related interannual Pacific SST variability perturbs the Pacific Walker circulation and thereby affects convective activity over the monsoon entrance region, thus modulating the isotopic composition of South American monsoon precipitation. This ENSO teleconnection has remained stationary over the last 120 years, regardless of the phase of the IPO.

While a number of studies document Pacific multidecadal variability, much of this work has drawn on basin-wide evidence to develop SST reconstructions and examines hydroclimate impacts as a secondary goal (D'Arrigo et al., 2001; Porter et al., 2021) or focuses on hydroclimate impacts from a precipitation lens (Dong et al., 2018; He et al., 2021). Prior to this study, to our knowledge, the mechanisms of how the IPO signal influences $\delta^{18}\text{O}$ variability in tropical South American records has not been documented in detail. Here, we show that at least some South American proxy records are characterized by statistically significant differences in their isotopic composition depending on the phase of the IPO and that they are significantly correlated with the IPO index. The sign and spatial pattern of the correlation with the IPO is consistent with the ENSO response, but with a reduced amplitude of the isotopic anomalies (Figure 3) and the atmospheric circulation response (Figures 6 and 7). This muted response to the IPO as compared to the ENSO forcing is consistent with prior studies that focused on the hydroclimate response to Pacific forcing, but without considering $\delta^{18}\text{O}_\text{p}$ (Flantua et al., 2016; Garreaud et al., 2009). Though the model captures a stronger signal in the ENSO composites, it nevertheless does validate the IPO response seen in the paleoclimate record and in GNIP observations. The broad agreement seen between proxies and model indicates the potential of the proxy records in archiving a low-frequency Pacific signal and paves the way for further proxy development to explore this teleconnection.

Low-frequency signals detected in proxy records from tropical South America in the past were commonly attributed to the AMO (Apaestegui et al., 2014; Chiessi et al., 2009; Novello et al., 2012), but our results show that the IPO must also be considered as a potential source of low-frequency variability for the South American monsoon domain. The AMO is postulated here to play a role in modulating the ENSO/IPO-SASM teleconnections based on current literature (He et al., 2021; Kayano & Capistrano, 2014), but a joint analysis of the interactions between all modes is needed to generate a quantitative attribution for how low-frequency forcing of the Atlantic versus Pacific influences the isotopic composition of precipitation over the South American monsoon domain. Additionally, the frequency characteristics of ENSO itself should be considered, particularly the multidecadal periods of low- and high-frequency El Niño/La Niña oscillations. The regional ENSO relationship with tree-width records from the Altiplano region has been shown to vary in time, with 1930–1960 CE noted as a period of relatively low-frequency ENSO (Crispín-DelaCruz et al., 2022). Finally, while recent studies have analyzed the interactions between these low-frequency modes and precipitation over South America (e.g., He et al., 2021), the inclusion of stable oxygen isotope records in this analytical framework is necessary to fully characterize the hydroclimatic impact of these modes and compare them against historical records.

6. Conclusions

The use of oxygen isotopes in evaluating hydroclimate variability gives way to unique insights into the study of the South American monsoon. Processes by which the monsoon is modulated due to both low- and high-frequency forcing of IPO and ENSO, respectively, were investigated in the isotope-enabled model and found to be of similar character, though differing strength. We show for the first time the spatial extent and amplitude of IPO forcing on South American $\delta^{18}\text{O}_\text{p}$ variability. The Walker circulation responds directly to changes in Pacific SST anomalies and indirectly modulates SASM convection on high- and low-frequency timescales. These findings are derived from isotope-enabled model simulations as well as terrestrial proxy records over the last century and IAEA-GNIP station observations over the past few decades. The model shows fidelity in reproducing the signal archived in the proxy records; both in terms of spatial extent and the magnitude of the $\delta^{18}\text{O}_\text{p}$ response to Pacific forcing. IAEA station data provide valuable support for interpreting model-proxy discrepancies and support regional conclusions, highlighting the value of this observational network and continued need for maintaining this data resource. The validation of the iCAM5 model with observations and proxy records supports its use for the interpretation of proxy records on multidecadal to interannual timescales. Though the internal variability inherent to a single model simulation precludes a detailed geographic investigation, the basis for comparison with paleoclimate records is sufficient to yield new and exciting results. As new records are developed, this work can be used as a point of reference to interpret stable oxygen isotope records as having either

a positive or negative relationships with the IPO and ENSO modes, as well as some estimation of the expected amplitude of the proxy response to these forcings.

Data Availability Statement

Paleoclimate records from PIM4 and JAR4 are available at the PANGEA data server: <https://www.pangaea.de/>. Paleoclimate records from Pumacocha, P00-H1, DV2+TR5+LD12, Quelccaya, and UTU are available at the NOAA Paleo Data website: <https://www.ncie.noaa.gov/access/paleo-search/>. Paleoclimate records from Cuy and Bol are available at <https://zenodo.org/record/7105508>. The SBE3 and JAR4 records can be found in the supplementary information of Novello et al. (2018). The MFZ-N-1 paleoclimate record is available pending data set publication. The Hadley-OI SST data can be accessed at https://gdex.ucar.edu/dataset/158_asphilli.html. GNIP isotope and precipitation data are available at <https://nucleus.iaea.org/wiser>. GPCC monthly 0.5° data is available at <https://www.dwd.de/EN/ourservices/gpcc/gpcc.html>. For this study, Global Precipitation Climatology Center (GPCC) data were provided by the NOAA PSL, Boulder, Colorado, USA, from their website at <https://psl.noaa.gov>. The AMO index (10-year lowpass) timeseries derived from the HadISST1 is available at <https://climatedataguide.ucar.edu/climate-data/atlantic-multi-decadal-oscillation-amo>. All analysis and figures were generated using Python. The code is available at <https://doi.org/10.5281/zenodo.11212407> (Orrison, 2024).

Acknowledgments

The authors would like to acknowledge this work as a product of the PIRE-CREATE project, which has enabled this vital international collaboration and cross-disciplinary research as well as those scholars whose efforts in the field and lab produced valuable proxy data that enabled this study. This work was made possible by funding from NSF for RO (OISE-1743738) and MV (OISE-1743738 and EAR-2103041). Funding from the São Paulo Research Foundation—FAPESP provided support for JCR (2019/02791-1), FC (2022/08359-7), and NMS (PIRE-CREATE project 2017/50085-3). NMS received additional support from the Conselho Nacional de Desenvolvimento Científico e Tecnológico—CNPq (312343/2022-1). The work of LA-H and MR-C was also supported by the project THEMES (Foundation BNP Paribas Climate Initiative program), the NSF projects OISE-1743738 and AGS-1702789, and the Lamont-Doherty Earth Observatory Climate Center. LA-H was partly funded by the NSF AGS-1903687. I. T. Pedron funded the collection and dating of the MFZ stalagmite (CNPq Grant: 426258/2016-9)). Finally, the authors would like to thank three anonymous reviewers whose comments helped improve the initial manuscript.

References

- Andreoli, R. V., & Kayano, M. T. (2005). ENSO-related rainfall anomalies in South America and associated circulation features during warm and cold Pacific decadal oscillation regimes. *International Journal of Climatology*, 25(15), 2017–2030. <https://doi.org/10.1002/joc.1222>
- Apáestegui, J., Cruz, F. W., Sifeddine, A., Vuille, M., Espinoza, J. C., Guyot, J. L., et al. (2014). Hydroclimate variability of the northwestern Amazon Basin near the Andean foothills of Peru related to the South American Monsoon System during the last 1600 years. *Climate of the Past*, 10(6), 1967–1981. <https://doi.org/10.5194/cp-10-1967-2014>
- Atwood, A. R., Battisti, D. S., Wu, E., Frierson, D. M. W., & Sachs, J. P. (2021). Data-model comparisons of tropical hydroclimate changes over the common era. *Paleoceanography and Paleoclimatology*, 36(7). <https://doi.org/10.1029/2020PA003934>
- Baker, J. C. A., Cintra, B. B. L., Gloor, M., Boom, A., Neill, D., Clerici, S., et al. (2022). The changing Amazon hydrological cycle—Inferences from over 200 years of tree-ring oxygen isotope data. *Journal of Geophysical Research: Biogeosciences*, 127(10), e2022JG006955. <https://doi.org/10.1029/2022JG006955>
- Bird, B. W., Abbott, M. B., Vuille, M., Rodbell, D. T., Stansell, N. D., & Rosenmeier, M. F. (2011). A 2,300-year-long annually resolved record of the South American summer monsoon from the Peruvian Andes. *Proceedings of the National Academy of Sciences of the United States of America*, 108(21), 8583–8588. <https://doi.org/10.1073/pnas.1003719108>
- Bradley, R. S., Vuille, M., Hardy, D., & Thompson, L. G. (2003). Low latitude ice cores record Pacific sea surface temperatures. *Geophysical Research Letters*, 30(4), 2002GL016546. <https://doi.org/10.1029/2002GL016546>
- Buckley, B. M., Ummenhofer, C. C., D'Arrigo, R. D., Hansen, K. G., Truong, L. H., Le, C. N., & Stahle, D. K. (2019). Interdecadal Pacific Oscillation reconstructed from trans-Pacific tree rings: 1350–2004 CE. *Climate Dynamics*, 53(5–6), 3181–3196. <https://doi.org/10.1007/s00382-019-04694-4>
- Cai, W., McPhaden, M. J., Grimm, A. M., Rodrigues, R. R., Taschetto, A. S., Garreaud, R. D., et al. (2020). Climate impacts of the El Niño–Southern Oscillation on South America. *Nature Reviews Earth and Environment*, 1(4), 215–231. <https://doi.org/10.1038/s43017-020-0040-3>
- Campos, J. L. P. S., Cruz, F. W., Ambrizzi, T., Deininger, M., Vuille, M., Novello, V. F., & Strikis, N. M. (2019). Coherent South American monsoon variability during the last millennium revealed through high-resolution proxy records. *Geophysical Research Letters*, 46(14), 8261–8270. <https://doi.org/10.1029/2019GL082513>
- Cauhy Rodrigues, J., Schulz, D., Vonhof, H., Strikis, N. M., Cruz, F. W., & Libera, M. E. D. (2022). Holocene extreme precipitation frequency and paleoclimate reconstruction based on high-resolution multi-proxy records from speleothems from south-east Brazil. In *Paper Presented at the AGU Fall Meeting*. Retrieved from <https://agu.confex.com/agu/fm22/meetingapp.cgi/Paper/1113680>
- Chen, T. C., Weng, S. P., & Schubert, S. (1999). Maintenance of austral summertime upper-tropospheric circulation over tropical South America: The Bolivian High-Nordeste Low system. *Journal of the Atmospheric Sciences*, 56(13), 2081–2100. [https://doi.org/10.1175/1520-0469\(1999\)056<2081:MOASUT>2.0.CO;2](https://doi.org/10.1175/1520-0469(1999)056<2081:MOASUT>2.0.CO;2)
- Chiessi, C. M., Mulitza, S., Pätzold, J., Wefer, G., & Marengo, J. A. (2009). Possible impact of the Atlantic multidecadal oscillation on the South American summer monsoon. *Geophysical Research Letters*, 36(21), 2009GL039914. <https://doi.org/10.1029/2009GL039914>
- Crispín-DelaCruz, D. B., Morales, M. S., Andreu-Hayles, L., Christie, D. A., Guerra, A., & Requena-Rojas, E. J. (2022). High ENSO sensitivity in tree rings from a northern population of *Polylepis tarapacana* in the Peruvian Andes. *Dendrochronologia*, 71, 125902. <https://doi.org/10.1016/j.dendro.2021.125902>
- Cruz, F. W., Karmann, I., Viana, O., Burns, S. J., Ferrari, J. A., Vuille, M., et al. (2005). Stable isotope study of cave percolation waters in subtropical Brazil: Implications for paleoclimate inferences from speleothems. *Chemical Geology*, 220(3–4), 245–262. <https://doi.org/10.1016/j.chemgeo.2005.04.001>
- Cruz, F. W., Vuille, M., Burns, S. J., Wang, X., Cheng, H., Werner, M., et al. (2009). Orbitally driven east–west antiphasing of South American precipitation. *Nature Geoscience*, 2(3), 210–214. <https://doi.org/10.1038/ngeo444>
- D'Arrigo, R., Villalba, R., & Wiles, G. (2001). Tree-ring estimates of Pacific decadal climate variability. *Climate Dynamics*, 18(3–4), 219–224. <https://doi.org/10.1007/s003820100177>
- Dee, S. G., Nusbaumer, J., Bailey, A., Russell, J. M., Lee, J.-E., Konecky, B., et al. (2018). Tracking the strength of the walker circulation with stable isotopes in water vapor: Water isotopes in vapor and global warming. *Journal of Geophysical Research: Atmospheres*, 123(14), 7254–7270. <https://doi.org/10.1029/2017JD027915>

- Della Libera, M. E., Novello, V. F., Cruz, F. W., Orrison, R., Vuille, M., Maezumi, S. Y., et al. (2022). Paleoclimatic and paleoenvironmental changes in Amazonian lowlands over the last three millennia. *Quaternary Science Reviews*, 279, 107383. <https://doi.org/10.1016/j.quascirev.2022.107383>
- Dong, B., Dai, A., Vuille, M., & Timm, O. E. (2018). Asymmetric modulation of ENSO teleconnections by the interdecadal Pacific oscillation. *Journal of Climate*, 31(18), 7337–7361. <https://doi.org/10.1175/JCLI-D-17-0663.1>
- Evans, M. N., Tolwinski-Ward, S. E., Thompson, D. M., & Anchukaitis, K. J. (2013). Applications of proxy system modeling in high resolution paleoclimatology. *Quaternary Science Reviews*, 76, 16–28. <https://doi.org/10.1016/j.quascirev.2013.05.024>
- Falster, G., Konecky, B., Madhavan, M., Stevenson, S., & Coats, S. (2021). Imprint of the Pacific walker circulation in global precipitation $\delta^{18}\text{O}$. *Journal of Climate*, 34(21), 8579–8597. <https://doi.org/10.1175/JCLI-D-21-0190.1>
- Facullo, J. T., Phillips, A. S., & Deser, C. (2020). Evaluation of leading modes of climate variability in the CMIP archives. *Journal of Climate*, 33(13), 5527–5545. <https://doi.org/10.1175/JCLI-D-19-1024.1>
- Fiorella, R. P., Poulsen, C. J., Pilco Zolá, R. S., Barnes, J. B., Tabor, C. R., & Ehlers, T. A. (2015). Spatiotemporal variability of modern precipitation $\delta^{18}\text{O}$ in the central Andes and implications for paleoclimate and paleoaltimetry estimates. *Journal of Geophysical Research: Atmospheres*, 120(10), 4630–4656. <https://doi.org/10.1002/2014JD022893>
- Fiorella, R. P., Siler, N., Nusbaumer, J., & Noone, D. C. (2021). Enhancing understanding of the hydrological cycle via pairing of process-oriented and isotope ratio tracers. *Journal of Advances in Modeling Earth Systems*, 13(10), e2021MS002648. <https://doi.org/10.1029/2021MS002648>
- Flantua, S. G. A., Hooghiemstra, H., Vuille, M., Behling, H., Carson, J. F., Gosling, W. D., et al. (2016). Climate variability and human impact in South America during the last 2000 years: Synthesis and perspectives from pollen records. *Climate of the Past*, 12(2), 483–523. <https://doi.org/10.5194/cp-12-483-2016>
- Galewsky, J., Steen-Larsen, H. C., Field, R. D., Worden, J., Risi, C., & Schneider, M. (2016). Stable isotopes in atmospheric water vapor and applications to the hydrologic cycle. *Reviews of Geophysics*, 54(4), 809–865. <https://doi.org/10.1002/2015RG000512>
- Garreaud, R. D., Vuille, M., Compagnucci, R., & Marengo, J. (2009). Present-day South American climate. *Palaeogeography, Palaeoclimatology, Palaeoecology*, 287(3–4), 180–195. <https://doi.org/10.1016/j.palaeo.2007.10.032>
- Grimm, A. M. (2003). The El Niño impact on the summer monsoon in Brazil: Regional processes versus remote influences. *Journal of Climate*, 16(2), 263–280. [https://doi.org/10.1175/1520-0442\(2003\)016<0263:TENIOT>2.0.CO;2](https://doi.org/10.1175/1520-0442(2003)016<0263:TENIOT>2.0.CO;2)
- He, Z., Dai, A., & Vuille, M. (2021). The joint impacts of Atlantic and Pacific multidecadal variability on South American precipitation and temperature. *Journal of Climate*, 34(19), 7959–7981. <https://doi.org/10.1175/JCLI-D-21-0081.1>
- Henley, B. J., Gergis, J., Karoly, D. J., Power, S., Kennedy, J., & Folland, C. K. (2015). A Tripole index for the interdecadal Pacific oscillation. *Climate Dynamics*, 45(11–12), 3077–3090. <https://doi.org/10.1007/s00382-015-2525-1>
- Hurley, J. V., Vuille, M., & Hardy, D. R. (2019). On the interpretation of the ENSO signal embedded in the stable isotopic composition of Quelccaya Ice Cap, Peru. *Journal of Geophysical Research: Atmospheres*, 124(1), 131–145. <https://doi.org/10.1029/2018JD029064>
- Hurrell, J. W., Hack, J. J., Shea, D., Caron, J. M., & Rosinski, J. (2008). A new sea surface temperature and sea ice boundary dataset for the community atmosphere model. *Journal of Climate*, 21(19), 5145–5153. <https://doi.org/10.1175/2008JCLI2292.1>
- IAEA/WMO. (2023). *Global network of isotopes in precipitation*. The GNIP Database. Retrieved from <https://nucleus.iaea.org/wiser/index.aspx>
- Insel, N., Poulsen, C. J., Sturm, C., & Ehlers, T. A. (2013). Climate controls on Andean precipitation $\delta^{18}\text{O}$ interannual variability. *Journal of Geophysical Research: Atmospheres*, 118(17), 9721–9742. <https://doi.org/10.1029/jgrd.5061>
- Kanner, L. C., Burns, S. J., Cheng, H., Edwards, R. L., & Vuille, M. (2013). High-resolution variability of the South American summer monsoon over the last seven millennia: Insights from a speleothem record from the central Peruvian Andes. *Quaternary Science Reviews*, 75, 1–10. <https://doi.org/10.1016/j.quascirev.2013.05.008>
- Kayano, M. T., & Capistrano, V. B. (2014). How the Atlantic multidecadal oscillation (AMO) modifies the ENSO influence on the South American rainfall. *International Journal of Climatology*, 34(1), 162–178. <https://doi.org/10.1002/joc.3674>
- Lacour, J.-L., Risi, C., Worden, J., Clerbaux, C., & Coheur, P.-F. (2018). Importance of depth and intensity of convection on the isotopic composition of water vapor as seen from IASI and TES 8D observations. *Earth and Planetary Science Letters*, 481, 387–394. <https://doi.org/10.1016/j.epsl.2017.10.048>
- Lenters, J. D., & Cook, K. H. (1997). On the origin of the Bolivian high and related circulation features of the South American climate. *Journal of the Atmospheric Sciences*, 54(5), 656–678. [https://doi.org/10.1175/1520-0469\(1997\)054<0656:OTOOTB>2.0.CO;2](https://doi.org/10.1175/1520-0469(1997)054<0656:OTOOTB>2.0.CO;2)
- Marengo, J. A., & Espinoza, J. C. (2016). Extreme seasonal droughts and floods in Amazonia: Causes, trends and impacts. *International Journal of Climatology*, 36(3), 1033–1050. <https://doi.org/10.1002/joc.4420>
- Marengo, J. A., Liebmann, B., Grimm, A. M., Misra, V., Silva Dias, P. L., Cavalcanti, I. F. A., et al. (2012). Recent developments on the South American monsoon system. *International Journal of Climatology*, 32(1), 1–21. <https://doi.org/10.1002/joc.2254>
- McCarroll, D., & Loader, N. J. (2004). Stable isotopes in tree rings. *Quaternary Science Reviews*, 23(7–8), 771–801. <https://doi.org/10.1016/j.quascirev.2003.06.017>
- Meehl, G. A., Hu, A., Castruccio, F., England, M. H., Bates, S. C., Danabasoglu, G., et al. (2021). Atlantic and Pacific tropics connected by mutually interactive decadal-timescale processes. *Nature Geoscience*, 14(1), 36–42. <https://doi.org/10.1038/s41561-020-00669-x>
- Midhun, M., Stevenson, S., & Cole, J. E. (2021). Oxygen isotopic signatures of major climate modes and implications for detectability in speleothems. *Geophysical Research Letters*, 48(1), e2020GL089515. <https://doi.org/10.1029/2020GL089515>
- Moore, M., Kuang, Z., & Blossey, P. N. (2014). A moisture budget perspective of the amount effect. *Geophysical Research Letters*, 41(4), 1329–1335. <https://doi.org/10.1002/2013GL058302>
- Moquet, J. S., Cruz, F. W., Novello, V. F., Strikis, N. M., Deininger, M., Karmann, I., et al. (2016). Calibration of speleothem $\delta^{18}\text{O}$ records against hydroclimate instrumental records in Central Brazil. *Global and Planetary Change*, 139, 151–164. <https://doi.org/10.1016/j.gloplacha.2016.02.001>
- Novello, V. F., Cruz, F. W., Karmann, I., Burns, S. J., Strikis, N. M., Vuille, M., et al. (2012). Multidecadal climate variability in Brazil's Nordeste during the last 3000 years based on speleothem isotope records. *Geophysical Research Letters*, 39(23), L23706. <https://doi.org/10.1029/2012GL053936>
- Novello, V. F., Cruz, F. W., Moquet, J. S., Vuille, M., de Paula, M. S., Nunes, D., et al. (2018). Two millennia of South Atlantic convergence zone variability reconstructed from isotopic proxies. *Geophysical Research Letters*, 45(10), 5045–5051. <https://doi.org/10.1029/2017GL076838>
- Nusbaumer, J., Wong, T. E., Bardeen, C., & Noone, D. (2017). Evaluating hydrological processes in the Community Atmosphere Model Version 5 (CAM5) using stable isotope ratios of water. *Journal of Advances in Modeling Earth Systems*, 9(2), 949–977. <https://doi.org/10.1002/2016MS000839>
- Orrison, R. (2024). Pacific influence on d18O in South American Monsoon precipitation [Software]. Zenodo. <https://doi.org/10.5281/zenodo.11212407>

- Orrison, R., Vuille, M., Smerdon, J. E., Apaéstegui, J., Azevedo, V., Campos, J. L. P. S., et al. (2022). South American Summer Monsoon variability over the last millennium in paleoclimate records and isotope-enabled climate models. *Climate of the Past*, 18(9), 2045–2062. <https://doi.org/10.5194/cp-18-2045-2022>
- Porter, S. E., Mosley-Thompson, E., Thompson, L. G., & Wilson, A. B. (2021). Reconstructing an interdecadal Pacific oscillation index from a Pacific basin-wide collection of ice core records. *Journal of Climate*, 34(10), 3839–3852. <https://doi.org/10.1175/JCLI-D-20-0455.1>
- Risi, C., Bony, S., & Vimeux, F. (2008). Influence of convective processes on the isotopic composition ($\delta^{18}\text{O}$ and δD) of precipitation and water vapor in the tropics: 2. Physical interpretation of the amount effect. *Journal of Geophysical Research*, 113(D19), D19306. <https://doi.org/10.1029/2008JD009943>
- Rodriguez-Catón, M., Andreu-Hayles, L., Daux, V., Vuille, M., Varuolo-Clarke, A. M., Oelkers, R., et al. (2022). Hydroclimate and ENSO variability recorded by oxygen isotopes from tree rings in the South American Altiplano. *Geophysical Research Letters*, 49(4). <https://doi.org/10.1029/2021GL095883>
- Rodriguez-Catón, M., Andreu-Hayles, L., Morales, M. S., Daux, V., Christie, D. A., Coopman, R. E., et al. (2021). Different climate sensitivity for radial growth, but uniform for tree-ring stable isotopes along an aridity gradient in *Polyplepis tarapacana*, the world's highest elevation tree species. *Tree Physiology*, 41(8), 1353–1371. <https://doi.org/10.1093/treephys/tpab021>
- Rodriguez-Catón, M., Morales, M. S., Rao, M. P., Nixon, T., Vuille, M., Rivera, J. A., et al. (2024). A 300-year tree-ring $\delta^{18}\text{O}$ -based precipitation reconstruction for the South American Altiplano highlights decadal hydroclimate teleconnections. *Communications Earth & Environment*, 5(1), 269. <https://doi.org/10.1038/s43247-024-01385-9>
- Ronchail, J., Cochonneau, G., Molinier, M., Guyot, J.-L., De Miranda Chaves, A. G., Guimarães, V., & de Oliveira, E. (2002). Interannual rainfall variability in the Amazon basin and sea-surface temperatures in the equatorial Pacific and the tropical Atlantic Oceans. *International Journal of Climatology*, 22(13), 1663–1686. <https://doi.org/10.1002/joc.815>
- Samuels-Crow, K. E., Galewsky, J., Hardy, D. R., Sharp, Z. D., Worden, J., & Braun, C. (2014). Upwind convective influences on the isotopic composition of atmospheric water vapor over the tropical Andes. *Journal of Geophysical Research: Atmospheres*, 119(12), 7051–7063. <https://doi.org/10.1002/2014JD021487>
- Schneider, U., Becker, A., Finger, P., Meyer-Christoffer, A., Rudolf, B., & Ziese, M. (2011). GPCC full data reanalysis version 6.0 at 0.5°: Monthly land-surface precipitation from rain-Gauges built on GTS-based and historic data. https://doi.org/10.5676/DWD_GPCC/FD_M_V7_050
- Schulman, E. (1956). *Dendroclimatic changes in semiarid America*. University of Arizona Press.
- Silva, M. E. S., Silva, C. B., Ambrizzi, T., Drumond, A., & Patucci, N. N. (2020). South America climate during the 1970–2001 Pacific decadal oscillation phases based on different reanalysis datasets. *Frontiers in Earth Science*, 7, 359. <https://doi.org/10.3389/feart.2019.00359>
- Steinman, B. A., Stansell, N. D., Mann, M. E., Cooke, C. A., Abbott, M. B., Vuille, M., et al. (2022). Interhemispheric antiphasing of neotropical precipitation during the past millennium. *Proceedings of the National Academy of Sciences of the United States of America*, 119(17), e2120015119. <https://doi.org/10.1073/pnas.2120015119>
- Sulca, J. (2021). Evidence of nonlinear Walker circulation feedbacks on extreme El Niño Pacific diversity: Observations and CMIP5 models. *International Journal of Climatology*, 41(5), 2934–2961. <https://doi.org/10.1002/joc.6998>
- Sulca, J., Takahashi, K., Espinoza, J., Vuille, M., & Lavado-Casimiro, W. (2018). Impacts of different ENSO flavors and tropical Pacific convection variability (ITCZ, SPCZ) on austral summer rainfall in South America, with a focus on Peru. *International Journal of Climatology*, 38(1), 420–435. <https://doi.org/10.1002/joc.5185>
- Sulca, J., Vuille, M., Silva, Y., & Takahashi, K. (2016). Teleconnections between the Peruvian central Andes and Northeast Brazil during extreme rainfall events in austral summer. *Journal of Hydrometeorology*, 17(2), 499–515. <https://doi.org/10.1175/JHM-D-15-0034.1>
- Thompson, L. G., Mosley-Thompson, E., Davis, M. E., Zagorodnov, V. S., Howat, I. M., Mikhalenko, V. N., & Lin, P.-N. (2013). Annually resolved ice core records of tropical climate variability over the past ~1800 years. *Science*, 340(6135), 945–950. <https://doi.org/10.1126/science.1234210>
- Trenberth, K. E., & Shea, D. J. (2006). Atlantic hurricanes and natural variability in 2005. *Geophysical Research Letters*, 33(12), 2006GL026894. <https://doi.org/10.1029/2006GL026894>
- Vance, T. R., Kiem, A. S., Jong, L. M., Roberts, J. L., Plummer, C. T., Moy, A. D., et al. (2022). Pacific decadal variability over the last 2000 years and implications for climatic risk. *Communications Earth & Environment*, 3(1), 33. <https://doi.org/10.1038/s43247-022-00359-z>
- Vera, C., Higgins, W., Amador, J., Ambrizzi, T., Garreaud, R., Gochis, D., et al. (2006). Toward a unified view of the American monsoon systems. *Journal of Climate*, 19(20), 4977–5000. <https://doi.org/10.1175/JCLI3896.1>
- Vuille, M., Bradley, R. S., Healy, R., Werner, M., Hardy, D. R., Thompson, L. G., & Keimig, F. (2003). Modeling $\delta^{18}\text{O}$ in precipitation over the tropical Americas: 2. Simulation of the stable isotope signal in Andean ice cores. *Journal of Geophysical Research*, 108(D6), 2001JD002039. <https://doi.org/10.1029/2001JD002039>
- Vuille, M., Bradley, R. S., Werner, M., Healy, R., & Keimig, F. (2003). Modeling $\delta^{18}\text{O}$ in precipitation over the tropical Americas: 1. Interannual variability and climatic controls. *Journal of Geophysical Research*, 108(D6), 2001JD002038. <https://doi.org/10.1029/2001JD002038>
- Vuille, M., Burns, S. J., Taylor, B. L., Cruz, F. W., Bird, B. W., Abbott, M. B., et al. (2012). A review of the South American monsoon history as recorded in stable isotopic proxies over the past two millennia. *Climate of the Past*, 8(4), 1309–1321. <https://doi.org/10.5194/cp-8-1309-2012>
- Vuille, M., & Werner, M. (2005). Stable isotopes in precipitation recording South American summer monsoon and ENSO variability: Observations and model results. *Climate Dynamics*, 25(4), 401–413. <https://doi.org/10.1007/s00382-005-0049-9>
- Wong, T. E., Nusbaumer, J., & Noone, D. C. (2017). Evaluation of modeled land-atmosphere exchanges with a comprehensive water isotope fractionation scheme in version 4 of the Community Land Model. *Journal of Advances in Modeling Earth Systems*, 9(2), 978–1001. <https://doi.org/10.1002/2016MS000842>
- Yasunaka, S., & Hanawa, K. (2011). Intercomparison of historical sea surface temperature datasets. *International Journal of Climatology*, 31(7), 1056–1073. <https://doi.org/10.1002/joc.2104>